

Compression and acceleration processes of spherical shells in gold cones

Huigang Wei^{1,5}, Dawei Yuan^{1,5}, Shaojun Wang², Ye Cui³, Xiaohu Yang^{3,5},
Yanyun Ma^{3,5}, Zhe Zhang^{2,5}, Xiaohui Yuan^{4,5}, Jiayong Zhong^{5,6}, Neng Hua⁷,
Yutong Li^{2,5,8*}, Jianqiang Zhu⁷, Gang Zhao^{1,9} and Jie Zhang^{2,4,5*}

¹ CAS Key Laboratory of Optical Astronomy, National Astronomical Observatories,
Chinese Academy of Sciences, Beijing 100101, China

² Beijing National Laboratory for Condensed Matter Physics, Institute of Physics,
Chinese Academy of Sciences, Beijing 100190, China

³ Department of Nuclear Science and Technology, National University of Defense
Technology, Changsha 410073, People's Republic of China

⁴ Key Laboratory for Laser Plasmas and School of Physics and Astronomy, and

⁵ Collaborative Innovation Center of IFSA (CICIFSA), Shanghai Jiao Tong University,
Shanghai 200240, People's Republic of China

⁶ Department of Astronomy, Beijing Normal University, Beijing 100875, China

⁷ National Laboratory on High Power Laser and Physics, Chinese Academy of
Sciences, Shanghai 201800, China

⁸ School of Physical Sciences, University of Chinese Academy of Sciences,
100049 Beijing, China

⁹ School of Astronomy and Space Science, University of Chinese Academy of Sciences,
Beijing 101408, China

This peer-reviewed article has been accepted for publication but not yet copyedited or typeset, and so may be subject to change during the production process. The article is considered published and may be cited using its DOI.

This is an Open Access article, distributed under the terms of the Creative Commons Attribution licence (<https://creativecommons.org/licenses/by/4.0/>), which permits unrestricted re-use, distribution, and reproduction in any medium, provided the original work is properly cited.

10.1017/hpl.2024.24

*Correspondence to: Yutong Li, Beijing National Laboratory for Condensed Matter Physics, Institute of Physics, Chinese Academy of Sciences, Beijing 100190, China. Email: ytli@iphy.ac.cn; Jie Zhang, Key Laboratory for Laser Plasmas (MOE) and School of Physics and Astronomy, Shanghai Jiao Tong University, Shanghai 200240, China. Email: jzhang1@sjtu.edu.cn

Abstract Double cone ignition (DCI) [Zhang et al., Phil. Trans. R. Soc. A 378: 20200015 (2020)] was proposed recently as a novel path for direct-drive inertial confinement fusion (ICF) using high power lasers. In this scheme, plasma jets with both high density and high velocity are required for collisions. Here we report preliminary experimental results obtained at the Shenguang-II upgrade laser facility, employing a CHCl shell in a gold cone irradiated with a two-ramp laser pulse. The CHCl shell was pre-compressed by the first laser ramp to a density of 3.75 g/cm^3 along the isentropic path. Subsequently, the target was further compressed and accelerated by the second laser ramp in the cone. According to the simulations, the plasma jet reached a density of up to 15 g/cm^3 , while measurements indicated a velocity of $126.8 \pm 17.1 \text{ km/s}$. The good agreements between experimental data and simulations are documented.

Key words: laser-plasma; double-cone ignition; compression and burn

I. INTRODUCTION

Significant progress has been made in both direct-drive[1,2] and indirect drive[3,4,5] inertial confinement fusion (ICF), while large challenges[6] still exist. Hence alternative paths, such as shock ignition[7], fast ignition[8], magneto-inertial fusion[9], are being explored. A novel ignition scheme, double cone ignition (DCI)[10], was recently proposed. Two fuel shells in two head-on gold cones are ablated by focused laser beams to compress the fuel up to 200 g/cm³ and then accelerated it to a velocity of more than 200 km/s. The pre-compressed plasma jets from the two cones collide to convert the kinetic energies to internal energy in the colliding plasma with higher density for fast ignition by fast electrons. Details of the discussions on these four processes can be found in the above paper.

In this paper, we mainly focus on the first two processes, namely compression and acceleration. The first process aims to pre-compress the shell to a high density before imploding the two shells with high velocities. To achieve this goal, multiple shocks are designed to precisely compress the target shell adiabatically, along the quasi-isentropic line. (However, the isentropic compression here is very short compared with the common isentropic process and is similar to shock compression. Thus we also use the shock compression to qualify this process.) This would significantly reduce the laser energy needed for implosion. The shocks finally coalesce at the rear surface of the shell, and the accurately timed coalescence of shocks is vital for a high quality compression. Previous experiments[11,12] were conducted on shock tuning at NIF and the compression of fuel was increased by a factor of 3 by finely tuning the arriving time of different shocks when comparing to the previous untuned results. For DCI, the second process is to accelerate the target to a high velocity after compressing it to high density. Thus, the laser pulse must be specially designed to achieve this goal.

Here we report the progress of shock experiments performed at the SGII-U laser facility[13]. The initial steps were aimed at studying the compression and acceleration of the outgoing jet in a single cone. It was a proof-of-principle experiment to confirm the feasibility of the first two processes for the DCI scheme. Future experiments will be performed with hundreds of kJ laser energy and double cones. In the present experiment, convergent compression waves generated by the two-ramp laser pulse were employed to compress the spherical CHCl shell. The laser pulse with two ramps was optimized for the CHCl shells in the gold cones to generate the jets with both high density and high velocity. As a preparation experiment, a two-ramp pulse, which will ultimately be optimized to a real isentropic laser pulse in future experiments, with a small slope in the first ramp was used to launch a quasi-isentropic compression on the target. This design aims to ensure that the shell follows the isentropic compression, achieving highest accessible density before being propelled to the highest accessible velocity. The energy distribution in the two ramps of the pulse was carefully designed to achieve this objective. The experiments conducted here are used to investigate the properties of the generated plasma jets from the cones. Optical diagnostics were used to measure the shock velocity in the CHCl shells, and the experimental results were carefully compared with 2-D simulations. This is the first one of a series of shock experiments for the DCI campaigns.

II. EXPERIMENTAL SETUP

The Shenguang II upgraded (SGII-U) laser facility, which can operate 8 beams with 1500 joules each at a wavelength of 351 nm, was employed to perform the experiment. The energy balance of the laser beams is less than 10%. Figure 1 represents the schematic experimental setup. The profile of each laser beam was temporally shaped into a two-ramp pulse, as shown in Fig.1. The first ramp pulse started with a step and had a rise time of 2.5 ns, intended to generate a fluid phase behind the shock in the CH shell and subsequently compress the shell

along the isentropic path. The second ramp pulse, with a rise time of 2 ns and a max intensity 140 times greater than that of the first pulse, was used to further compress and accelerate the target. The laser beams were focused to a spot with a 2 mm diameter flat top profile using a continuous phase plate (CPP). For comparison, some shots with the rectangle pulse were also conducted.

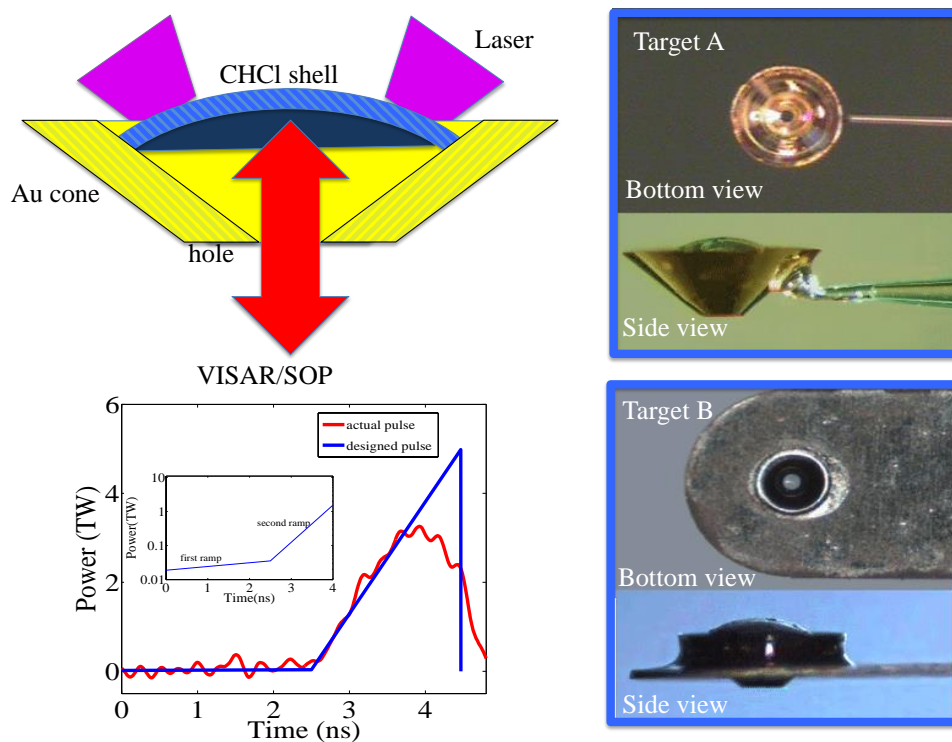


Figure 1. Sketch of the experimental setup with the two-ramp pulse profile and the targets. Four laser beams irradiate the CHCl shell targets. A probe laser penetrates the hole of the Au cone and is reflected back by the shock into the VISAR diagnostics. The target self-emissions are measured by SOP.

As the initial step for the DCI scheme, the plasma jets at the cone tips should be carefully characterized before collisions, hence only one cone with a shell target was used. Cl-doped polystyrene (CH) was chosen as the shell to improve direct-drive implosion performance[14], meanwhile, chlorine was used as a trace element for other diagnostics. Helium-like triplets from Cl were measured by the X-ray spectrometer and used to determine the plasma densities and temperatures[15]. The shell was shaped into a spherical cap with a cap angle of

50° and a sphere inner radius of 250 μm , which was glued to the wall of the gold cone. The shell was irradiated by four laser beam with intensities up to $4.6 \times 10^{15} \text{ W/cm}^2$. The thickness of the shell was 50 μm . The experiment setup is presented in Fig.1, where the cone was glued to a thin glass pole (Target A) or supported by an Al plate with a hole (Target B). To avoid blocking the instruments to diagnose the jet, type-A targets were used, otherwise type-B targets were used as type-A targets were prone to damage. The shocks generated in the shell strengthen with increased laser intensity. Consequently, the latter shocks propagate faster than the former ones and coalesce at the rear surface of the CHCl shell with the first shock. The CHCl plasma is propelled forward and out of the gold cone through the hole at the tip of the cone. As the CHCl plasma moves forward, it undergoes further compression by the wall of the gold cone.

The shock velocity propagated in the CHCl shell was measured through the hole of the gold cone by the velocity interferometry system for any reflector (VISAR)[16], which utilizes a 50 ns pulse width probe laser[17]. A 15 mm etalon was used, corresponding to a velocity sensitivity of 4.288 km/s/fringe. An optical fiducial was added to the streak camera to provide absolute timing. The CHCl target has a low reflection for the VISAR probe at 660 nm, and no signal is detected from the CHCl shell through the cone hole before the main laser ablation. The reflector in this experiment is the shock front in the CHCl shell, which can be considered as the beginning of the laser pulse since the shock are formed rapidly when the laser ablates the CHCl shell. The Streaked Optical Pyrometer (SOP) was employed as a complementary diagnostic to measure the emission of shocks in the CHCl shell.

III. EXPERIMENTAL RESULTS AND SIMULATIONS

Figure 2 shows the measured VISAR images for a typical rectangle pulse shot [Fig. 2(b)] together with the results for a two-ramp pulse shot [Fig. 2(c)]. The horizontal direction of these images corresponds to the spatial direction

transverse to the shock velocity, while time increases from top to bottom. Fig. 2(a) shows the reference image for target A without the main laser pulses, where only the bright fringes of the VISAR laser beam reflected by the wall surface at the tip of the gold cone can be detected. The fringes corresponding to the stationary CHCl shell were too weak to be detected since most of the VISAR laser passes through the CHCl shell. The laser energy for rectangle pulse was 5.6 kJ with a pulse duration of 2 ns. Simulations showed that a pulse of 2 ns is a preferable choice, which can drive the jet to eject from the tip of the cone near the end of the laser pulse. This can efficiently convert the laser energy to the jet kinetic energy for rectangle pulse. Due to the malfunction of the laser cooling system during the experiments, a relatively stronger pre-pulse was observed before the main pulse. This pre-pulse irradiated the front surface of the transparent CHCl shell and caused an increased reflection efficiency of the VISAR laser beam. Consequently, relatively dark fringes can be observed from the CHCl shell before the arrival of the main pulse, $t = 0$ ns, in Fig. 2(b). When the main pulse arrived, the shock in the CHCl shell became a reflector, and the signal of fringes increased abruptly. After the main pulse, at $t = 0.51$ ns, the VISAR signal disappeared as the shock broke out at the rear surface and released into the vacuum. This indicates a shock velocity of 98 km/s.

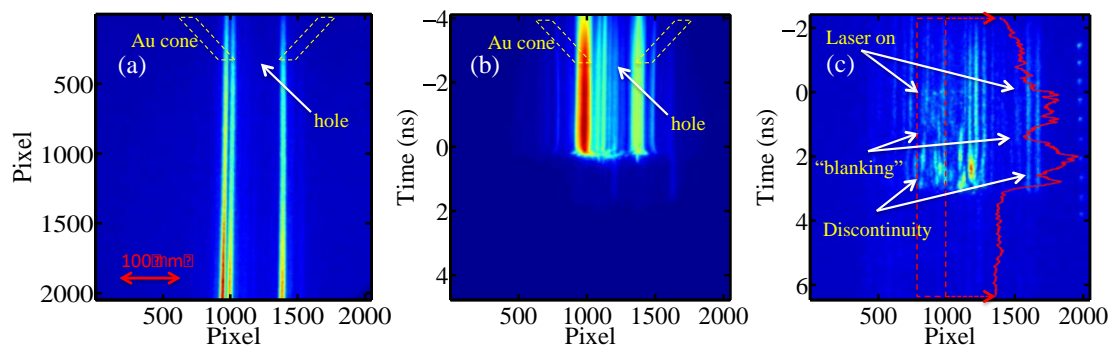


Figure 2. VISAR images for rectangle pulse and two-ramp pulse shots. (a) The reference image of target A without the laser shot. (b) The VISAR image for the rectangle pulse shot with target A. (c) The VISAR image for the two-ramp pulse shot with target B. The red line is the temporal intensities of VISAR fringes extracted from the dashed rectangle box.

For comparison, Fig. 2(c) shows the VISAR result for the two-ramp pulse

shot, along with the temporal intensities of VISAR fringes. Before $t = 0$ ns, the relatively bright fringes represent reflections of VISAR probe laser from the wall at the cone tip and the supporting Al plate (see target B in Fig.1). Similar to the rectangle pulse case, the weak fringes at the cone hole can be observed by the reflection of the coarse surface of the CHCl shell due to the pre-pulse before the two-ramp pulse. From $t = 0$ ns, the main pulse irradiates the CHCl shell and forms shocks within it, and the fringes reflecting from these shocks can be clearly observed. Unlike the rectangle pulse case, the fringes in this two-ramp shot last for 3.1 ns before disappearing. This is because the first ramp pulse is much weaker than the rectangle pulse, resulting in weaker shocks that propagate slower. This ramp compresses the shell close to an isentropic compression. When the first ramp pulse arrives at $t = 0$ ns, the increase in the fringe intensity indicates the formation of a shock reflector. The weak fringe signals caused by the beginning of the first ramp pulse suggest that the initial shocks may still be nearly transparent for the probe laser beam. From 0 ns to 3.1 ns, the temporal rise in signal intensity suggests that the shocks are getting stronger with time, thus the reflectivity for the probe laser beam becomes larger[18]. The VISAR blanking observed at around 1.0 ns may be due to either the photoionization of the target material ahead of the shock by the x-rays from the ablation corona[19] or the CHCl material being compressed to a state which turns optically opaque to the probing laser[20]. At 2.5 ns, the second ramp pulse irradiates the target and causes a short discontinuity in the fringes. At 3.1 ns, the sudden increase in fringe signals indicates that the shocks generated by the second ramp pulse overtake the former shocks generated by the first ramp pulse and break out at the rear surface of CHCl shell, which then causes the fringes disappearing. This agrees with the simulation well (see below) and suggests that the CHCl shell undergoes a quasi-isentropic compression before being accelerated as a whole by the later ramp.

Temporal emissions from the shock in the CHCl shell, measured with the SOP,

are shown in Fig. 3(a), together with the cartoon of the gold cone indicating the corresponding spatial locations. The horizontal direction corresponds to the time, increasing from left to right. Initially, the emission is observed to be well collimated. As time increases, the spatial size of the emission increases, and the intensity also strengthens. The full widths at half maximum (FWHM) of the emission source are plotted in Fig. 3(b) as a function of time. The FWHM of the source is $100 \pm 5 \mu\text{m}$ from $t = 2.95 \text{ ns}$ to $t = 4.59 \text{ ns}$. This is identical to the diameter of the cone tip hole ($100 \mu\text{m}$), indicating that the plasma is inside the cone. The starting time ($t = 2.95 \text{ ns}$) for this constant FWHM also serves as a cross-check of the VISAR results for the time when the shocks break out at the rear surface of the shell. A sharp increase in the FWHM can be seen from $t = 4.59 \text{ ns}$, followed by a quick decrease in less than 1 ns. This is because the SOP records mainly the emissions from the tip cone hole before $t = 4.59 \text{ ns}$ and from the expanding plasmas passing through of the cone's tip hole after $t = 4.59 \text{ ns}$. By combining the expanding spatial distance and the travel time, the expansion speed of the plasmas can be estimated to be $126.8 \pm 17.1 \text{ km/s}$. This speed is in agreement with the results from x-ray pinhole streak camera (XPSC) [21]. A similar jet with a velocity of about 600 km/s was reported[22] at a laser intensity of 700 TW/cm^2 .

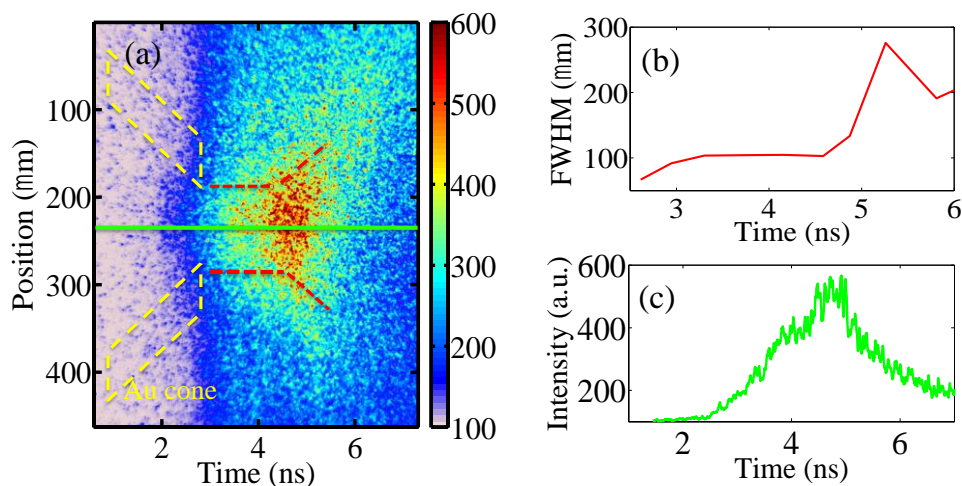


Figure 3. SOP signals of the two-ramp shot. (a) Streaked image of emissions, with a cartoon of gold cone shown to indicate

the corresponding locations. (b) Temporal FWHM of emission source. (c) Lineout along the central axis of CHCl shell in SOP image.

Emission signals along the central axis of the CHCl shell are extracted and shown in Fig. 3(c). Starting from 1.45 ns, an emission signal appears in the SOP record, albeit at the same level as the background. The steady increase in emission implies a gradual strengthening of the shock over time. This is consistent with the VISAR results, where increased shocks are also observed. Emission signals from the strong shocks generated by the second ramp become clearly distinguishable from 2.5 ns onward. Although these strong shocks have not overtaken those of the first ramp at that time, their emissions can penetrate through the preceding shocks, which are not fully opaque. Rare signals are detected from the shocks generated by the first ramp suggesting that the compression is along an isentropic path. This self-emission reaches its max value at 4.91 ns.

Experimental results are simulated with the two-dimensional cylindrical hydrodynamic code FLASH[23,24], which includes radiation transport, electron thermal conduction, laser energy deposition and three-temperature model. The simulation results are shown in Figure 4. The laser energy is 5 kJ, with a wavelength of 0.351 μm and a spot radius of 250 μm , the same as the experimental designed conditions. In the simulations, the laser propagates along the cone wall and focuses at the top of CH target. The input parameters are the exact experimental designed conditions for laser and target, with the exception that the simulations employ a CH target due to lack of opacity data for the CHCl targets. The MPQEOS equations of state[25] and the SNOP opacity tables[26] are used for the CH target. The target has an inner radius of 250 μm and a thickness of 50 μm , as shown in Fig. 4(a).

The simulation results for the rectangle pulse are shown in Fig. 4(a) and 4(b). The shock positions are clearly discernible by the steepest gradient density distributions. At $t = 0.589$ ns, the shock reaches the rear surface of the CH shell,

indicating that the VISAR signals will soon disappear. This time (0.589 ns) is in good agreement with our experimental results, where the fringes disappear at 0.51 ns, considering the experimental uncertainties (± 100 ps). In the simulations of the two-ramp pulse shot, shown in Fig. 4(c)-4(f), the first ramp pulse is relatively weak, causing the shock to propagate more slowly in the CH shell compared to the rectangle shot. The first shock reaches the rear surface of the shell at $t = 2.55$ ns (Fig. 4(c)), and the strong shocks start to form due to ablation by the second ramp. This corresponds with the records from SOP, where strong signals are detected starting at $t = 2.5$ ns. These strong shocks break out at the rear surface of CH shell at 3.05 ns in the simulation (Fig. 4(d)), coinciding with experimental measurement by VISAR (3.1 ns). The VISAR record disappears at 3.1 ns, making it impossible to gain information from this optical diagnostic beyond this point. Fortunately, the SOP results continue to provide insights into the evolution of plasma both inside and outside the gold cone. The plasmas begin to emerge from the tip hole of the cone at 4.45 ns and subsequently expand freely, as shown in Fig. 4(f). This agrees well with the SOP results, which shows a sharp increase in the FWHM of the source size from $t = 4.59$ ns. As we compared above, the time differences between the simulation results and the measurements obtained by VISAR and SOP are no more than 150 ps. While this value is slightly larger than the experiment errors (± 100 ps), it is noteworthy that the experimental laser power is smaller than the designed pulse power. Consequently, the plasmas take more time to emerge from the tip hole in the experiment than in the simulations in which the designed laser shape is used. Considering this respect, we believe that the agreement between the simulations and the experimental measurements is reasonable.

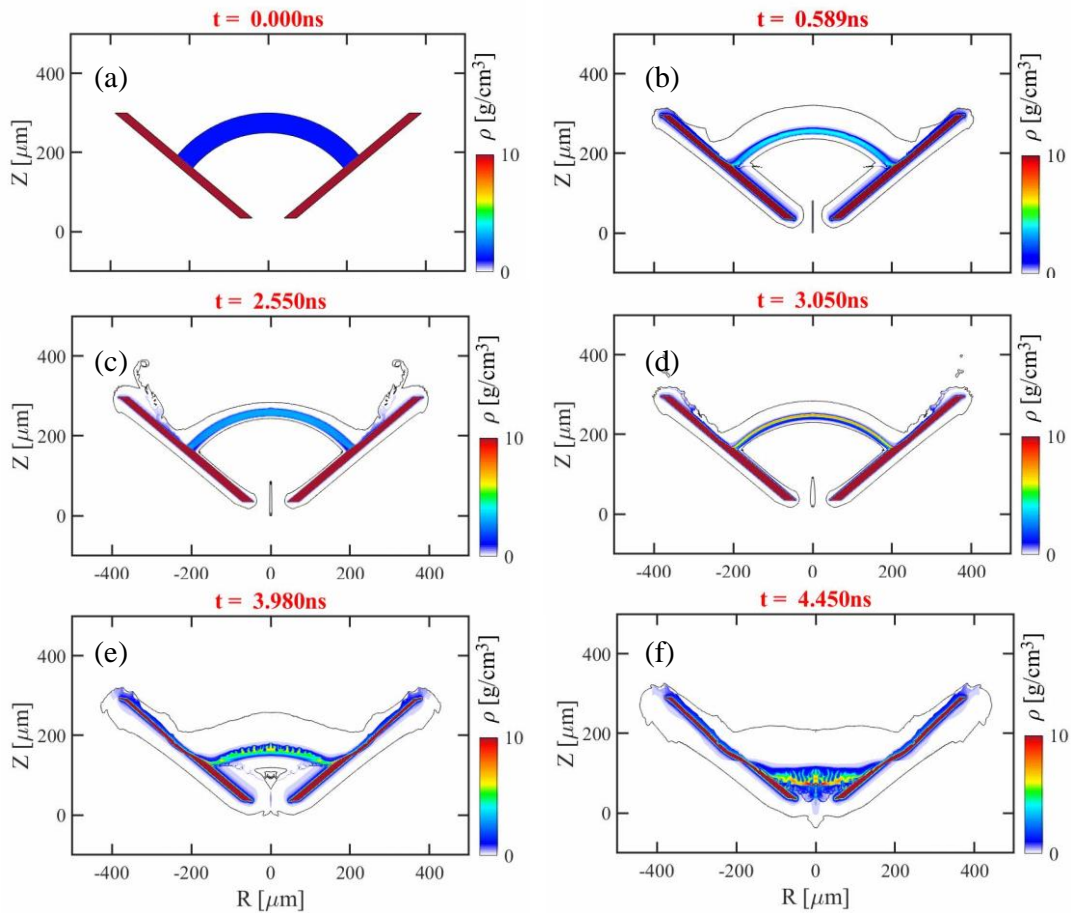


Figure 4. Temporal density distributions in CHCl shell. (a)-(b), Simulation of density distribution in CHCl shell for rectangle pulse shot at $t = 0$ ns and $t = 0.589$ ns. (c)-(f), Simulation of density distribution in CHCl shell for two-ramp pulse shot from $t = 2.550$ ns to $t = 4.450$ ns.

Figure 5 shows the simulated density distributions along the axis of the CH shell targets at different times. From $t = 0$ to $t = 2.55$ ns, the CH shell is compressed by the shocks from the first ramp pulse. As time increases, the CH shell is fully compressed to a density of 3.75 g/cm³ by the end of the first pulse. Essentially, this process is the same as a typical spherical convergence, where the CH shell is compressed by converging shock waves (CSW). The trajectory of the CSW can be well described by the Chester–Chisnell–Whitham (CCW) method[27]. In the strong shock limit, this method is in a good agreement with the Guderley theory[28]: $\frac{R}{R_0} = \left(1 - \frac{t}{t_0}\right)^n$, where R_0 is the shock initial position, t_0 is the arrival time at the center of the shell, and n is the similarity exponent, related to

the adiabatic exponent γ . Simulations shown in fig. 6 plot the normalized converging shock positions against the normalized time relative to the arrival time at the shell center in a log-log coordinate system. The slope of the linear fit to this line gives the similarity exponent, $n = 0.798$, in Guderley formula. In spherical shocks, this similarity exponent corresponds to the adiabatic exponent $\gamma = 1.10$ for ideal gas[29]. Solids with a Grüneisen parameter Γ_0 behave similarly to the gas with the adiabatic exponent $\gamma = \Gamma_0 + 1$ [30]. Based on this, the Grüneisen parameter was calculated for CH shell, yielding a value of $\Gamma_0 = 0.10$. This value is less than commonly reference data[31]. However, recent calculations and experimental measurements on CH/GDP[32,33] suggest that the Grüneisen parameter is less than 0.2 at low densities, which are in good agreement with our results. The peak density of 3.75 g/cm³ in our spherical compression by the first ramp is also higher than the density (less than 3.5 g/cm³) in planar compression[34], indicating that the shock strengthens in converging process.

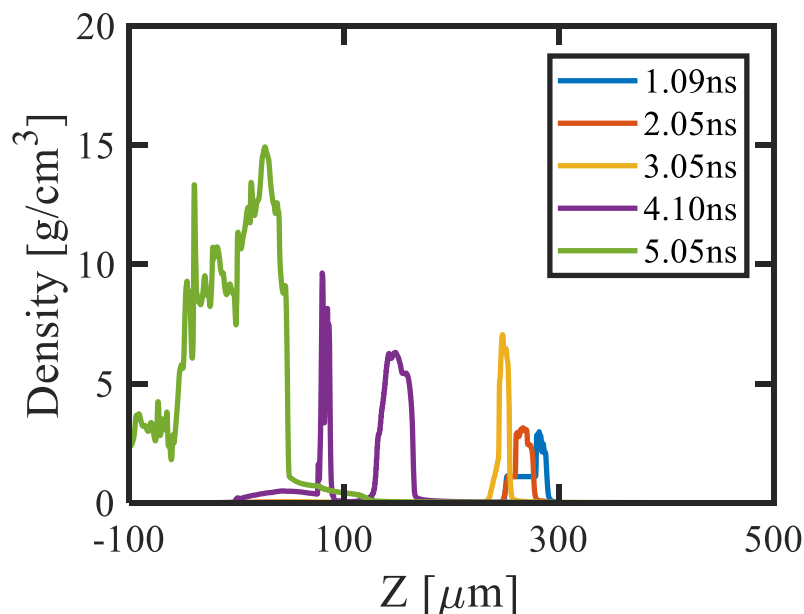


Figure 5. The density along the target axis at different times for the two-ramp pulse shot.

After the first ramp, shocks generated by the second ramp uniformly compress this pre-compressed CH shell to a density as high as 7.5 g/cm³ at 3.05 ns, indicating that these strong shocks reach the rear surface of the CH.

Subsequently, the entire CH shell is accelerated forward and simultaneously compressed by the pressure from both the laser ablation and the squeeze from the wall of gold cone as it moves toward the tip of the cone. This process is three-dimensional. With the driven laser on, the densities of the CH shell remain almost constant (7.5 g/cm^3), while the thickness of the shell increases again since its spherical radius decreases when approaching the tip of the cone, shown in Fig. 5 at 4.1 ns. At the end of the driven laser ($t = 4.5 \text{ ns}$), the central part of the CH shell continues to move at high speed, while the marginal parts move more slowly due to the expansion of the cone wall into the cone, which prevents direct interaction of the laser pulse with the margin of CH shell, and also due to the drag of the inner wall of the gold cone. Consequently, the CH shell becomes flattened, as shown in Fig. 4(f). A high-density plasma jet forms due to inertia of the shell. Upon collision between the marginal parts of CH shell and the cone wall, a recoil force further compresses the jet as it moves toward the cone tip. The highest density of 14.92 g/cm^3 is achieved at $t = 5.05 \text{ ns}$, represented by the green line in Fig.5. Since the emission is proportional to the density of the plasma, this is also in agreement with the SOP measurements, which show the strongest emission at $t = 4.91 \text{ ns}$. Thus, we have shown that with the gold cone, a high-density jet with high velocity can be produced. The gold cone plays an important role in containing and compressing the plasma jet before the jet ejects from the tip hole.

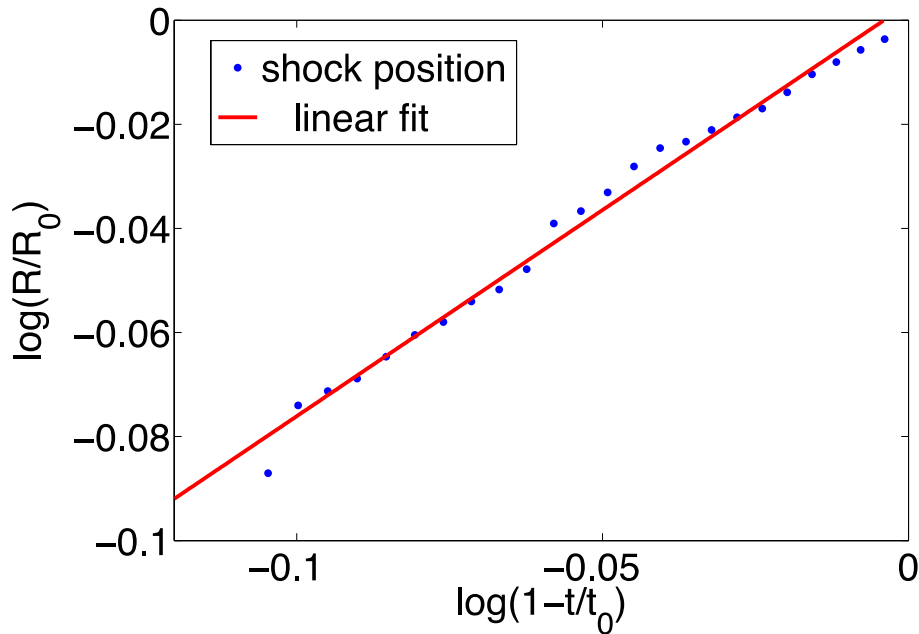


Figure 6. Converging shock positions versus the time in our simulations. The blue dots are normalized shock positions and the red line is the linear fit.

IV. SUMMARY AND CONCLUSIONS

The CHCl shell in the gold cone was irradiated by a specially designed laser shape, namely the two-ramp pulse. The shocks generated by the first ramp fulfilled the quasi-isentropic compression of the target. Subsequent shocks generated by the second ramp further compressed and accelerated the shell to generate a high-density jet with high velocity. The shock velocity profiles in the CH shell were measured by VISAR, while the emissions from the shocks were recorded by SOP. The steady increase in the intensity of both the VISAR fringes and the SOP signals indicates that shocks grew stronger as they propagated through the CH shell. The measured arrival times of shocks at the rear surface of the CH shell are in good agreement with the simulation results conducted by the hydrodynamic code FLASH, considering the experimental inaccuracies (± 100 ps). The plasma jet ejected from the tip hole of the gold cone and reached the maximum emission at the predicted times given by the code. Additionally, for shots with the rectangle laser pulse, the measured shocks with a velocity of 98

km/s were also well reproduced in the simulation results. This gives us confidence in the simulation results and demonstrates our ability to generate the required jet conditions under current laser conditions. The path through which converging shock transported in the CH shell agrees with Guderley's theory, showing the increasing shock strength. The CH plasma jet, driven by the ablation of the second ramp pulse in the gold cone, can reach a maximum density of 14.92 g/cm^3 according to simulations, with a velocity measured up to $126.8 \pm 17.1 \text{ km/s}$. In conclusion, generation of high-density and high-velocity plasma jets with a two-ramp pulse has been demonstrated experimentally in preliminary shock experiment for the DCI campaigns. The benchmarked code will be modified to optimize the experimental design, and new diagnostics are being developed for subsequent experiments with the upgrading laser system. These well-characterized jets will be used for the next steps of DCI campaigns, where the two jets will collide into each other and be trapped by external magnetic fields to prepare the necessary conditions for fast heating by fast electrons.

Acknowledgement

We thank all the staffs of the SGII-upgrade laser facility for the support of the experiment and the staffs of Shanghai institute of laser plasma and Shanghai Jiao Tong University for the target fabrication. This work is supported by the Strategic Priority Research Program of Chinese Academy of Sciences, Grant Nos.: XDA25030500 and XDA25050200, the National Natural Science Foundation of China under grant Nos. 11988101, 11890694, 12173058, 12175309, and the National Key R&D Program of China No. 2019YFA0405502.

Availability of data

Data available on request from the authors.

References

1. J. D. Lindl, "Development of the indirect-drive approach to inertial confinement fusion and the target physics basis for ignition and gain", *Phys. Plasmas* 2, 3933 (1995).
2. S. P. Regan, V. N. Goncharov, I. V. Igumenshchev, T. C. Sangster, R. Betti, A. Bose, T. R. Boehly, M. J. Bonino, E. M. Campbell, D. Cao, T. J. B. Collins, R. S. Craxton, A. K. Davis, J. A. Delettrez, D. H. Edgell, R. Epstein, C. J. Forrest, J. A. Frenje, D. H. Froula, M. Gatu Johnson, V. Yu Glebov, D. R. Harding, M. Hohenberger, S. X. Hu, D. Jacobs-Perkins, R. Janezic, M. Karasik, R. L. Keck, J. H. Kelly, T. J. Kessler, J. P. Knauer, T. Z. Kosc, S. J. Loucks, J. A. Marozas, F. J. Marshall, R. L. McCrory, P. W. McKenty, D. D. Meyerhofer, D. T. Michel, J. F. Myatt, S. P. Obenschain, R. D. Petrasso, P. B. Radha, B. Rice, M. J. Rosenberg, A. J. Schmitt, M. J. Schmitt, W. Seka, W. T. Shmayda, M. J. Shoup, A. Shvydky, S. Skupsky, A. A. Solodov, C. Stoeckl, W. Theobald, J. Ulreich, M. D. Wittman, K. M. Woo, B. Yaakobi, J. D. Zuegel, "Demonstration of Fuel Hot-Spot Pressure in Excess of 50 Gbar for Direct-Drive, Layered Deuterium-Tritium Implosions on OMEGA", *Phys. Rev. Lett.* 117, 025001 (2016).
3. J. D. Lindl, P. Amendt, R. L. Berger, S. G. Glendinning, S. H. Glenzer, S. W. Haan, R. L. Kauffman, O. L. Landen, and L. J. Suter, "The physics basis for ignition using indirect-drive targets on the National Ignition Facility", *Phys. Plasmas* 11, 339 (2004).
4. A. B. Zylstra, A. L. Kritcher, O. A. Hurricane, D. A. Callahan, K. Baker, T. Braun, D. T. Casey, D. Clark, K. Clark, T. Döppner, L. Divol, D. E. Hinkel, M. Hohenberger, C. Kong, O. L. Landen, A. Nikroo, A. Pak, P. Patel, J. E. Ralph, N. Rice, R. Tommasini, M. Schoff, M. Stadermann, D. Strozzi, C. Weber, C. Young, C. Wild, R. P. J. Town, and M. J. Edwards, "Record Energetics for an Inertial Fusion Implosion at NIF", *Phys. Rev. Lett.* 126, 025001 (2021).
5. O. A. Hurricane, D. A. Callahan, D. T. Casey, P. M. Celliers, C. Cerjan, E. L. Dewald, T. R. Dittrich, T. Döppner, D. E. Hinkel, L. F. Berzak Hopkins, J. L. Kline, S. Le

- Pape, T. Ma, A. G. MacPhee, J. L. Milovich, A. Pak, H.-S. Park, P. K. Patel, B. A. Remington, J. D. Salmonson, P. T. Springer and R. Tommasini, "Fuel gain exceeding unity in an inertially confined fusion implosion", *Nature* 506, 343 (2014).
6. R. Betti, O. Hurricane, "Inertial-confinement fusion with lasers", *Nature Phys.* 12, 435–448 (2016).
 7. R. Betti, C. D. Zhou, K. S. Anderson, L. J. Perkins, W. Theobald, and A. A. Solodov, "Shock Ignition of Thermonuclear Fuel with High Areal Density", *Phys. Rev. Lett.* 98, 155001 (2007).
 8. M. Tabak, J. Hammer, M. E. Glinsky, W. L. Kruer, S. C. Wilks, J. Woodworth, E. M. Campbell, M. D. Perry, and R. J. Mason, "Ignition and high gain with ultrapowerful lasers", *Phys. Plasmas* 1, 1626 (1994).
 9. S. A. Slutz, M. C. Herrmann, R. A. Vesey, A. B. Sefkow, D. B. Sinars, D. C. Rovang, K. J. Peterson, and M. E. Cuneo, "Pulsed-power-driven cylindrical liner implosions of laser preheated fuel magnetized with an axial field", *Phys. Plasmas* 17, 056303 (2010).
 10. J. Zhang, W. M. Wang, X. H. Yang, D. Wu, Y. Y. Ma, J. L. Jiao, Z. Zhang, F. Y. Wu, X. H. Yuan, Y. T. Li, J. Q. Zhu, "Double-cone ignition scheme for inertial confinement fusion", *Phil. Trans. R. Soc. A* 378: 20200015 (2020).
 11. H. F. Robey, P. M. Celliers, J. L. Kline, A. J. Mackinnon, T. R. Boehly, O. L. Landen, J. H. Eggert, D. Hicks, S. Le Pape, D. R. Farley, M. W. Bowers, K. G. Krauter, D. H. Munro, O. S. Jones, J. L. Milovich, D. Clark, B. K. Spears, R. P. J. Town, S. W. Haan, S. Dixit, M. B. Schneider, E. L. Dewald, K. Widmann, J. D. Moody, T. D€oppner, H. B. Radousky, A. Nikroo, J. J. Kroll, A. V. Hamza, J. B. Horner, S. D. Bhandarkar, E. Dzenitis, E. Alger, E. Giraldez, C. Castro, K. Moreno, C. Haynam, K. N. LaFortune, C. Widmayer, M. Shaw, K. Jancaitis, T. Parham, D. M. Holunga, C. F. Walters, B. Haid, T. Malsbury, D. Trummer, K. R. Coffee, B. Burr, L. V. Berzins, C. Choate, S. J. Brereton, S. Azevedo, H. Chandrasekaran, S. Glenzer, J. A. Caggiano, J. P. Knauer, J. A. Frenje, D. T. Casey, M. Gatu Johnson, F. H. Seguin, B. K. Young, M. J. Edwards, B. M. Van Wonterghem, J. Kilkenny, B. J. MacGowan, J. Atherton, J. D. Lindl, D. D. Meyerhofer, and E. Moses, "Precision Shock Tuning on the National

- Ignition Facility”, *Phys. Rev. Lett.* 108, 215004 (2012).
12. H. F. Robey, T. R. Boehly, P. M. Celliers, J. H. Eggert, D. Hicks, R. F. Smith, R. Collins, M. W. Bowers, K. G. Krauter, P. S. Datte, D. H. Munro, J. L. Milovich, O. S. Jones, P. A. Michel, C. A. Thomas, R. E. Olson, S. Pollaine, R. P. J. Town, S. Haan, D. Callahan, D. Clark, J. Edwards, J. L. Kline, S. Dixit, M. B. Schneider, E. L. Dewald, K. Widmann, J. D. Moody, T. Doppner, H. B. Radousky, A. Throop, D. Kalantar, P. DiNicola, A. Nikroo, J. J. Kroll, A. V. Hamza, J. B. Horner, S. D. Bhandarkar, E. Dzenitis, E. Alger, E. Giraldez, C. Castro, K. Moreno, C. Haynam, K. N. LaFortune, C. Widmayer, M. Shaw, K. Jancaitis, T. Parham, D. M. Holunga, C. F. Walters, B. Haid, E. R. Mapoles, J. Sater, C. R. Gibson, T. Malsbury, J. Fair, D. Trummer, K. R. Coffee, B. Burr, L. V. Berzins, C. Choate, S. J. Brereton, S. Azevedo, H. Chandrasekaran, D. C. Eder, N. D. Masters, A. C. Fisher, P. A. Sterne, B. K. Young, O. L. Landen, B. M. Van Wonterghem, B. J. MacGowan, J. Atherton, J. D. Lindl, D. D. Meyerhofer, and E. Moses, “Shock timing experiments on the National Ignition Facility: Initial results and comparison with simulation”, *Phys. Plasmas* 19, 042706 (2012).
13. J. Q. Zhu, J. Zhu, X. C. Li, B. Q. Zhu, W. X. Ma, X. Q. Lu, W. Fan, Z. G. Liu, S. L. Zhou, G. Xu, G. W. Zhang, X. L. Xie, L. Yang, J. F. Wang, X. P. Ouyang, L. Wang, D. W. Li, P. Q. Yang, Q. T. Fan, M. Y. Sun, C. Liu, D. A. Liu, Y. L. Zhang, H. Tao, M. Z. Sun, P. Zhu, B. Y. Wang, Z. Y. Jiao, L. Ren, D. Z. Liu, X. Jiao, H. B. Huang, and Z. Q. Lin, “Status and development of high-power laser facilities at the NLHPLP”, *High Power Laser Sci. Eng.* 6, e55 (2018).
14. G. N. Zheng, T. Tao, Q. Jia, R. Yan and J. Zheng, “Optimizing doping parameters of target to enhance direct-drive implosion”, *Plasma Phys. Control. Fusion* 64, 105003 (2022).
15. H. Liu, X. H. Yang, Y. H. Zhang, Y. Fang, Z. Zhang, X. H. Yuan, Y. T. li, and J. Zhang, “Demonstration of enhanced direct-drive implosion efficiency using gradient pulses”, *Phys. Rev. E.* 105, L053203 (2022).
16. D. W. Yuan, S. J. Wang, H. G. Wei, H. C. Gu, Y. Dai, J. Y. Zhong, Y. T. Li, G. Zhao, and J. Zhang, “Design, performance and application of a line-imaging velocity interferometer system for any reflector coupled with a streaked optical

- pyrometer system at the Shenguang-II upgrade laser facility”, *High Power Laser Sci. Eng.* 12, e6 (2024).
17. Q. Xiao, X. Pan, J. T. Guo, X. Q. Wang, J. F. Wang, X. Q. Jiang, G. Y. Li, X. H. Lu, X. C. Wang, S. L. Zhou, and X. C. Li, “High-stability, high-beam-quality, and pulse-width-tunable 1319 nm laser system for VISAR applications in high-power laser facilities”, *Appl. Opt.* 59, 6070 (2020).
 18. M. A. Barrios, D. G. Hicks, T. R. Boehly, D. E. Fratanduono, J. H. Eggert, P. M. Celliers, G. W. Collins, and D. D. Meyerhofer, “High-precision measurements of the equation of state of hydrocarbons at 1-10 Mbar using laser-driven shock waves”, *Phys. Plasmas* 17, 056307 (2010).
 19. S. Laffite, S. D. Baton, P. Combis, J. Clerouin, M. Koenig, V. Recoules, C. Rousseaux, and L. Videau, “Velocity Interferometer blanking due to preheating in a double pulse planar experiment”, *Phys. Plasmas* 21, 082705 (2014).
 20. N. J. Hartley, C. Zhang, X. Duan, L. G. Huang, S. Jiang, Y. Li, L. Yang, A. Pelka, Z. Wang, J. Yang, and D. Kraus, “Dynamically pre-compressed hydrocarbons studied by self-impedance mismatch”, *Matter Radiat. Extremes* 5, 028401 (2020).
 21. Z. Zhang, X. H. Yuan, Y. H. Zhang, H. Liu, K. Fang, C. L. Zhang, Z. D. Liu, X. Zhao, Q. L. Dong, G. Y. Liu, Y. Dai, H. C. Gu, Y. T. Li, J. Zheng, J. Y. Zhong, J. Zhang, “Efficient energy transition from kinetic to internal energy in supersonic collision of high-density plasma jets from conical implosions”, *Acta Physica Sinica* 71, 155201 (2022)
 22. H. Azechi, T. Sakaiya, T. Watari, M. Karasik, H. Saito, K. Ohtani, K. Takeda, H. Hosoda, H. Shiraga, M. Nakai, K. Shigemori, S. Fujioka, M. Murakami, H. Nagatomo, T. Johzaki, J. Gardner, D. G. Colombant, J. W. Bates, A. L. Velikovich, Y. Aglitskiy, J. Weaver, S. Obenschain, S. Eliezer, R. Kodama, T. Norimatsu, H. Fujita, K. Mima, and H. Kan, “Experimental Evidence of Impact Ignition: 100-Fold Increase of Neutron Yield by Impactor Collision”, *Phys. Rev. Lett.* 102, 235002 (2009).
 23. B. A. Fryxell, K. Olson, P. Ricker, F. X. Timmes, M. Zingale, D. Q. Lamb, P. MacNeice, R. Rosner, J. W. Truran, and H. Tufo, “FLASH: An Adaptive Mesh

- Hydrodynamics Code for Modeling Astrophysical Thermonuclear Flashes”, *Astrophys. J., Suppl.* 131, 273 (2000).
24. A. Dubey, K. Antypas, M. K. Ganapathy, L. B. Reid, K. Riley, D. Sheeler, A. Siegel, and K. Weide, “Extensible component-based architecture for FLASH, a massively parallel, multiphysics simulation code”, *Parallel Comp.* 35, 512 (2009).
25. A. J. Kemp and J. Meyer-ter-Vehn, “An equation of state code for hot dense matter, based on the QEOS description”, *Nucl. Instrum. Meth. Phys. Res. A* 415, 674 (1998).
26. K. Eidmann, “Radiation transport and atomic physics modeling in high-energy-density laser-produced plasmas”, *Laser Part. Beams* 12, 223 (1994).
27. G. B. Whitham, *Linear and Nonlinear Waves* (Wiley, New York, 1974), p. 263-311.
28. G. Guderley, “Starke kugelige und zylindrische Verdichtungsstöße in der Nähe des Kugelmittelpunktes bzw. der Zylinderachse”, *Luftfahrtforschung* 19, 302 (1942).
29. L. E. Bilbao and J. Gratton, “Spherical and cylindrical convergent shocks”, *IL Nuovo Cimento*, 18, 9, 1996.
30. Zeldovich and Y. P. Raizer, *Physics of shock waves and high temperature hydrodynamic phenomena* (New York: Academic Press 1966), p. 700.
31. M. A. Meyers, *Dynamic Behavior of Materials* (John Wiley & Sons, Inc. 1994), p. 128-133.
32. P. Colin-Lalu, V. Recoules, G. Salin, T. Plisson, E. Brambrink, T. Vinci, R. Bolis, and G. Huser, “Dissociation along the principal Hugoniot of the Laser Mégajoule ablator material”, *Phys. Rev. E* 94, 023204 (2016).
33. C. A. McCoy, S. X. Hu, M. C. Marshall, D. N. Polsin, D. E. Fratanduono, Y. H. Ding, P. M. Celliers, T. R. Boehly, and D. D. Meyerhofer, “Measurement of the sound velocity and Grüneisen parameter of polystyrene at inertial confinement fusion conditions”, *Phys. Rev. B* 102(18), 184102 (2020).
34. S.J. Wang, D. W. Yuan, H. G. Wei, F. Y. Wu, H. C. Gu, Y. Dai, Z. Zhang, X. H. Yuan,

Y. T. Li, and J. Zhang, "Interaction of multiple shocks in planar targets with a ramp-pulse ablation", *Phys. Plasmas* 29, 112701 (2022).